

# Quasicrystal model sets from overlapping self-similar attractors

Christoph Bandt and Yves Meyer

May 26, 2026

## Abstract

We give a simple computational approach to mathematical quasicrystals, combining cut-and-project methods with self-similarity. Starting with a Pisot unit  $\beta$  and an iterated function system  $g_k(z) = \beta z + z_k$ ,  $k = 1, \dots, m$  in a corresponding ring of algebraic integers, we take the attractor  $A$  of the conjugate system as an acceptance window. This yields the unique cut-and-project model set  $\Lambda$  in the complex plane which fulfils  $\Lambda = \bigcup g_k(\Lambda)$ .

We describe an algorithm which directly determines  $\Lambda$ , avoiding the difficulties with the fractal structure of  $A$ . Classical constructions are based on tiles  $A$  of different shape. The present study continues work on models with overlaps, as introduced by Gummelt (1996), Baake and Grimm (2013), Hejda and Pelantova (2016), and Hare, Masakova and Vavra (2018). In our approach, the overlaps provide a natural decoration of  $\Lambda$ . The method is illustrated with a variety of pentagonal examples.

## 1 Motivation

There are two main principles to construct Delone sets modelling quasicrystals: cut-and-project models and inflation procedures. Both were justified by physical experiments, and they can be combined. Many papers have studied the interplay of the two principles, cf. [3, 4, 14, 19, 22]. The recent work of Harriss, Koivusalo and Walton [15] summarizes a main connection in an abstract  $n$ -dimensional and multicolored setting as follows: *a cut-and-project set is substitutional if and only if its acceptance window has a self-similar structure.*

The present paper contains a more concrete statement for expanding iterated function systems (IFS) in the plane: *any IFS with a Pisot unit as factor has a unique cut-and-project set as its maximal solution within the corresponding ring of integers.* The only other condition is that the IFS contains enough maps to make its conjugate attractor plane-filling. The statement could be generalized to higher dimensions, using the concept of a Pisot family [19], to graph-directed IFS, and also to fractal patterns which are not relatively dense [6]. This note aims more at simplicity than generality, however. It arose from a search for models of decagonal quasicrystals which are simpler than the common Penrose tilings [4, 12, 25], or the version with overlapping Gummelt decagons often used by physicists [13, 27]. The ‘atomic positions’ shall be defined directly, without use of rotations and different types of tiles.

Let  $G = \{z^1, \dots, z^5\}$  be the set of fifth roots of unity. In a first approach, we studied the direct sum  $\Lambda_1 = \bigcup_{n=0}^{\infty} \sum_{k=0}^n \tau^k G$  where  $\tau = \frac{1+\sqrt{5}}{2}$ . From the viewpoint of numeration systems, the convex hull of  $G$ , shown in Figure 1, is the ‘unit interval’, and the digits are taken from  $G$ . This

was already done by Hare, Masakova and Vavra [14] who considered all sums  $z = \sum_{k=0}^n a_k \tau^k$  with  $n \in \mathbb{N}$  and digits  $a_k \in \{0\} \cup G$ . Both definitions lead to the set  $\Lambda_1$  shown in Figure 2a. It is a subset of a cut-and-project model set. However, it has to be complemented by the set  $\Lambda_2$  in Figure 2b in order to become the model set  $\Lambda^*$  in Figure 2c.

We shall give a straightforward construction for the model set of an arbitrary Pisot IFS, which allows to calculate many self-similar model sets. Over the years, physicists have synthesized about 100 stable quasicrystals [1, 20, 21, 27, 28], probably not all of equal importance. Mathematical models stick mainly to the Penrose family, or the Tübingen triangle tilings [4]. The algorithm presented here makes it possible to screen many self-similar model sets, most of which are probably not important. Actually, we were not sure whether the IFS approach provides patterns of the same quality as the use of tilings. We expected that with graph-directed IFS the Penrose patterns could be reproduced. It came as a surprise, however, that even the simplest ordinary IFS lead to several interesting and apparently new examples.

An IFS seems the most simple formal description of a self-similar model set. It is computer-accessible and for the plane requires less information than three lines of text. The atomic positions are fixed by the IFS. For our figures we could only choose the patch. As a rule, regions far from the origin provide more regular patches. The decoration for our figures is also defined by the IFS. We did only select the colors. The algorithm of this paper could be a step towards the establishment of computer-maintained databases of mathematical quasicrystals which would complement the beautiful tiling encyclopedia [11]. This requires other algorithms for the characterization, comparison and classification of patterns. Physicists do already use machine learning for the prediction of new quasicrystals [21].

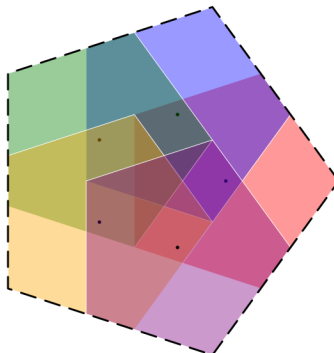


Figure 1: The pentagon is a typical overlapping self-similar set. Its geometry is crucial for our examples. Our basic example in Figure 2 will be derived from a conjugate attractor, however.

## 2 Overview

In the complex plane, we consider an iterated function system (IFS) of expanding functions

$$g_k(x) = \beta x + z_k, k = 1, \dots, m \tag{1}$$

where  $\beta$  is a real or complex Pisot unit, and both  $\beta$  and the  $z_k$  are integers in an algebraic field. There will be a conjugate IFS of contracting functions

$$g'_k(x) = \beta'x + z'_k. \quad (2)$$

A well-known theorem of Hutchinson [7, 8, 9] says that there is a unique nonempty compact attractor  $A$  defined by

$$A = \bigcup_{k=1}^m g'_k(A). \quad (3)$$

We shall consider an associated equation for discrete sets and the original expanding IFS.

$$\Lambda = \bigcup_{k=1}^m g_k(\Lambda). \quad (4)$$

Statements related to the following theorem are known from the literature, in particular for the octagonal case [3, 4, 14, 15, 16, 22]. We shall provide a new and astonishingly simple constructive approach. With  $\Lambda(W)$  we denote the model set for a window  $W$  in conjugate space. When  $W$  has interior points and the boundary of  $W$  has zero area, it is known that  $\Lambda(W)$  is a Meyer set and has pure point diffraction spectrum. These are the basic properties for quasicrystal modeling. Precise definitions will be introduced in the following sections.

**Theorem 1** *Consider an expanding IFS (1) where  $\beta$  is either a complex Pisot unit or a real Pisot unit with the condition (6) in a cyclotomic field. Let the  $z_k$  belong to the corresponding ring  $R$  of algebraic integers. Let  $A$  denote the attractor of the conjugate, contracting IFS (2), or in the case of several conjugates, the product of their attractors. Then every solution  $\Lambda \subset R$  of (4) is a subset of  $\Lambda(A)$ , and  $\Lambda^* = \Lambda(A)$  is the maximal solution of the equation (4) in  $R$ .*

This can be considered as a discrete counterpart of Hutchinson's theorem for attractors. The assumption of a Pisot number is natural since whenever  $g_1(\Lambda) \subseteq \Lambda$ , the expanding factor must be a Pisot or a Salem number [23, 10], and no solution of an equation (4) for a Salem factor has ever been found. We restrict ourselves to units since we use the inverse maps of the  $g_k$  in the sections 4 and 6.

Self-similarity has been frequently observed in physical quasicrystals [20, 25, 27]. Here its purpose is to determine  $\Lambda^*$  explicitly by recursion. We combine the cut-and-project method with self-similarity and circumvent the difficulties caused by the fractal structure of  $A$ .

For our pentagonal example,  $\beta = \tau$  and  $\beta' = -t = -1/\tau$ . The attractor of (2), drawn in Figure 3b in Section 8, contains the closed ball  $B$  of radius  $\tau$  around zero since  $B \subset \bigcup g'_k(B)$ . So  $A$  certainly has non-empty interior. The set  $\Lambda_1$  defined above and shown in Figure 2a is a Meyer set since  $\Lambda_1 \subset \Lambda(A)$ . However, as proved in [14, Section 4], it is not the model set of  $A$  - some points are missing. The missing points, however, form another Meyer set  $\Lambda_2$  depicted in Figure 2b. The union  $\Lambda_1 \cup \Lambda_2$  in Figure 2c is the model set  $\Lambda(A)$  which seems a more perfect and physically plausible quasicrystal model than  $\Lambda_1$ .

The attractors  $A$ , like Figure 1, have very heavy overlaps which obscure their structure. Probably for this reason tilings have been preferred in quasicrystal modelling. However, as

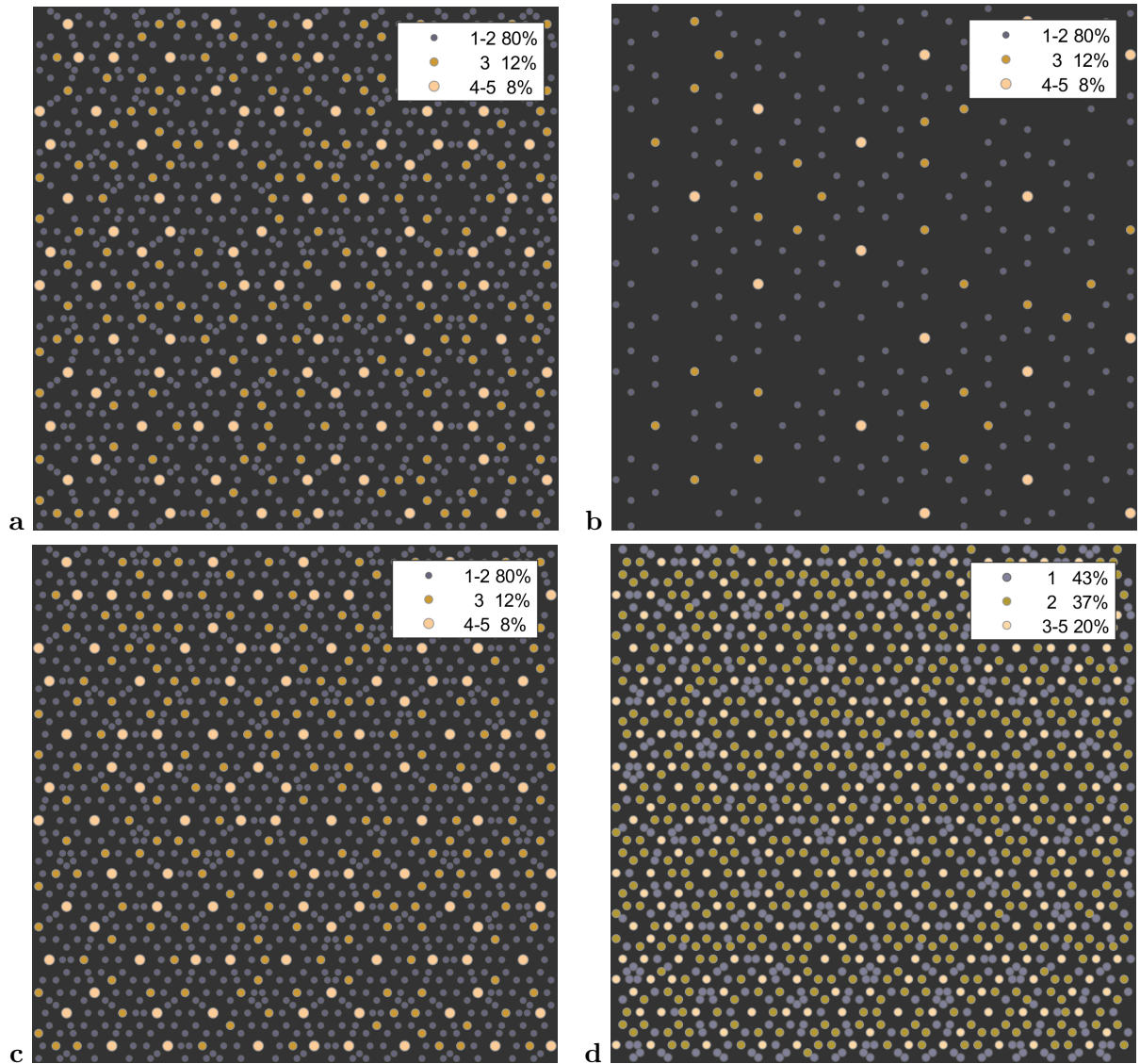


Figure 2: **a** and **b** are two solution sets of (4) for  $g_k(x) = \tau x + z^k$ ,  $k = 1, \dots, 5$  where  $z = \exp 2\pi i/5$ . Since  $-3 < x_1, x_2 < 12$ , the origin is near the lower left corner. **c** is the model set  $\Lambda(A)$  obtained as the union of **a** and **b**. In **d** this set is shown in a region away from zero,  $5 < x_1, x_2 < 20$ , with a slightly different decoration. The decoration is explained in Section 9.

noted by various authors [1, 13, 27, 28], from a physical viewpoint the formation of quasicrystals from overlapping clusters seems more plausible than the edge-to-edge fitting of tiles. Moreover, while heavy overlaps of attractors are a nightmare in fractal geometry, they do not form an obstacle in the study of discrete sets. When two points overlap, it is still one point. The overlaps even turn into a virtue when we use them to indicate the importance or stability of

an atom in the compound. The color and size of the atoms in Figure 2 were obtained from the number of immediate overlaps in the point. The frequencies and relative positions of different atoms are in rather close analogy to physical quasicrystals composed of different metallic atoms, cf. [2, 20, 27, 28].

In the sections 3 to 6, we introduce the basic concepts and prove Theorem 1. Section 7 describes the algorithmic construction. The pentagonal example of Figure 2 is treated in detail in Section 8. The natural decoration of the patterns is explained in Section 9. The last three sections discuss interesting examples.

### 3 Pisot factors and conjugacy

Let  $\beta$  be a real or complex Pisot unit. That is,  $\beta$  is a root of a polynomial  $p(z) = z^d + a_{d-1}z^{d-1} + \dots + a_1z + a_0$  with integer coefficients  $a_k$  and  $a_0 = \pm 1$  such that  $|\beta| > 1$  and all other roots  $\beta'$  of  $p$ , except for the complex-conjugate of  $\beta$ , have modulus smaller than 1. Our calculations are performed within the ring  $R$  of integers of a complex algebraic number field  $K$ .

**Complex Pisot numbers**  $\beta$ . In this case  $K$  is generated by  $\beta$ , and  $R = \mathbb{Z}[\beta]$ . The complex numbers  $1, \beta, \beta^2, \dots, \beta^{d-1}$  form a linear basis of  $R$ . Any point  $x \in R$  has a representation  $x = n_0 + n_1\beta + n_2\beta^2 + \dots + n_{d-1}\beta^{d-1}$  with  $n_k \in \mathbb{Z}$ . This defines a one-to-one mapping  $\pi : \mathbb{Z}^d \rightarrow R \subset \mathbb{C}$  with  $\pi(n) = x$  for  $n = (n_0, \dots, n_{d-1})$ .

For each conjugate root  $\beta'$  we have another basis  $1, \beta', \dots, (\beta')^{d-1}$  of  $R$  and another one-to-one projection  $\pi' : \mathbb{Z}^d \rightarrow \mathbb{C}$  with  $\pi'(n) = x' = n_0 + n_1\beta' + \dots + n_{d-1}(\beta')^{d-1}$ . There is a Galois automorphism  $\varphi : R \rightarrow R$  with  $\varphi(\beta) = \beta'$ . This mapping maps  $x$  to  $x'$ , it is the composition  $x' = \varphi(x) = \pi' \cdot \pi^{-1}(x)$ . In this section, we discuss the case of a single conjugate. The combination of several conjugates is treated in Section 6.

We have described the spaces of a cut-and-project scheme [4, 24, 25]. When we write the basis vectors  $1, \beta, \dots, \beta^{d-1}$  as a  $2 \times d$  real matrix  $B$  and the vectors of the conjugate basis  $1, \beta', \dots, (\beta')^{d-1}$  as another  $2 \times d$  matrix  $B'$ , and take  $n$  as a column vector  $n = (n_0, \dots, n_{d-1})^\top$ , the scheme is realized by matrix multiplication:

$$\pi : \mathbb{Z}^d \rightarrow \mathbb{C} \text{ with } \pi(n) = B \cdot n \text{ and } \pi' : \mathbb{Z}^d \rightarrow \mathbb{C} \text{ with } \pi'(n) = B' \cdot n.$$

This scheme can be numerically represented in a computer when we restrict ourselves to coordinates  $n_k$  with  $|n_k| \leq N$  for small  $N$ . Let

$$\mathbb{Z}_N^d = \{n = (n_0, \dots, n_{d-1})^\top \in \mathbb{Z}^d \mid -N \leq n_k \leq N \text{ for } k = 0, 1, \dots, d-1\}. \quad (5)$$

**Remark 2 (Numerical realization of the cut-and-project scheme)** *Multiplying  $B$  and  $B'$  with all column vectors  $n \in \mathbb{Z}_N^d$ , we obtain two matrices  $X$  and  $X'$  of shape  $2 \times (2N+1)^d$ . If  $x$  is the number in the  $k$ -th column of  $X$ , the  $k$ -th column of  $X'$  contains  $x' = \varphi(x)$ . In this way the matrices  $X, X'$  describe the correspondence  $\varphi$  between  $x = \pi(n)$  and  $x' = \pi'(n)$ . All examples of this paper can be derived from a single calculation of  $X$  and  $X'$  for  $N = 5$ .*

**Real Pisot numbers**  $\beta$ . We consider the cyclotomic field  $K$  generated by the  $n$ -th roots of unity,  $z^k, k = 0, 1, \dots, n-1$  with  $z = \cos \frac{2\pi}{n} + i \sin \frac{2\pi}{n}$ , and  $R = \mathbb{Z}[z]$ . In our examples we take

$\beta = (z + \bar{z}) + 1$  which is a Pisot number for  $n = 5, 7, 8$ , and  $12$ . The condition required for  $\beta$  is

$$\text{The only Galois automorphisms } \psi \text{ of } K \text{ with } \psi(\beta) = \beta \text{ are } \psi(x) = x \text{ and } \psi(x) = \bar{x}. \quad (6)$$

This implies  $|\beta'| < 1$  for all conjugates in  $K$ . The condition includes the Pisot-cyclotomic numbers, as defined in [14] and listed there in Table 1.

In the cyclotomic field, the Galois automorphisms  $\varphi : R \rightarrow R$  are defined by  $\varphi(z) = z^\ell$  where  $\ell$  is an integer between 1 and  $\frac{n}{2}$  such that the greatest common divisor  $\gcd(\ell, n)$  is 1. Then  $\beta' = \varphi(\beta) = (z^\ell + \bar{z}^\ell) + 1$  is a Galois conjugate of the Pisot number  $\beta$  and thus must have modulus smaller than 1. Remark 2 applies with basis matrices  $B$  and  $B'$  representing  $z, z^{m_2}, \dots, z^{m_d}$  and  $z^\ell, z^{m_2\ell}, \dots, z^{m_d\ell}$ . Here  $1, m_2, \dots, m_d$  denote the integers between 1 and  $n - 1$  with  $\gcd(m_k, n) = 1$ .

For the pentagon example  $n = 5$  and  $d = 4$ . Taking  $\ell = 2$ , the columns of the matrices  $B, B'$  are given by  $z, z^2, z^3, z^4$  and  $z^2, z^4, z, z^3$ , respectively.

## 4 The expanding IFS and self-similar discrete sets

Let  $\beta$  with  $|\beta| > 1$  and  $z_1, \dots, z_m$  belong to the ring  $R$  of algebraic integers. The Pisot property is not needed in this section. We consider the expanding IFS  $g_k(x) = \beta x + z_k$ ,  $k = 1, \dots, m$ . A point set  $\Lambda$  is called self-similar with respect to the IFS if

$$\Lambda = \bigcup_{k=1}^m g_k(\Lambda). \quad (4)$$

Any solution set must be infinite, and any union of solutions is a solution of (4). In general there are many solutions. The equation  $\Lambda = 2\Lambda \cup (2\Lambda - 1)$ , for instance, has as solutions on the real line the positive integers, the non-positive integers, all rationals, all rationals of the form  $k/p$  for any fixed prime number  $p$ , and so on.

When we ask for discrete solutions, however, there is a nice structure of solutions [5, 17, 29]. A closed set  $L$  in a metric space is *discrete* if each ball contains only finitely many points of  $L$ . In the sequel, we consider only closed and discrete solutions  $\Lambda$  of (4). A *cycle* of the IFS  $\{g_1, \dots, g_m\}$  is a set  $\{x_1, \dots, x_n\}$  such that there are indices  $j_1, \dots, j_n \in \{1, \dots, m\}$  with  $g_{j_k}(x_k) = x_{k+1}$  for  $k = 1, \dots, n - 1$  and  $g_{j_n}(x_n) = x_1$ . The following estimate shows that all cycles of the IFS lie in a fairly small ball. This is the starting point for our calculational approach.

**Lemma 3** *Let  $c = \frac{\max_j |z_j|}{|\beta| - 1}$ . Then  $|y| > c$  implies  $|g_k(y)| > |y|$  for  $k = 1, \dots, m$ .*

*Thus all cycles of the IFS  $\{g_1, \dots, g_m\}$  lie within the closed ball  $B_c(0)$  of radius  $c$  around zero.*

*Moreover,  $|y| > 2c$  implies  $|g_k^{-1}(y)| < |y| - \frac{\max |z_j|}{|\beta|}$  for  $k = 1, \dots, m$ .*

*Proof.*  $|y| > c$  means  $|y| \cdot |\beta| - \max |z_j| > |y|$ . Thus  $|g_k(y)| = |\beta y + z_k| \geq |\beta| \cdot |y| - |z_k| > |y|$ . Such  $y$  cannot belong to a cycle. For  $|y| > 2c$  we have  $|\beta| \cdot |y| - |y| > 2 \max |z_j|$ . Hence  $|g_k^{-1}(y)| = |(y - z_k)/\beta| < |y/\beta| + |z_k/\beta| < |y| - 2 \max |z_j|/|\beta| + |z_k|/|\beta|$ .  $\square$

**Proposition 4 (Basic properties of discrete self-similar sets [5, 17, 29])**

Let  $\{g_1, \dots, g_m\}$  be the expanding IFS (1) on  $\mathbb{C}$ , and let  $L \subset \mathbb{C}$  be a discrete closed set.

1. Any closed and discrete solution  $\Lambda$  of (4) must contain a cycle of the IFS.
2. Any closed and discrete solution of (4) is obtained from its cycles by repeated application of all the  $g_k$ .
3. The number of solutions within  $L$  is finite.
4. There is a unique maximal solution of (4) within  $L$ .
5. A point  $z \in L$  belongs to this maximal solution if and only if there are indices  $k_1, \dots, k_p \in \{1, \dots, m\}$  such that  $g_{k_p}^{-1} \cdots g_{k_1}^{-1}(z)$  belongs to a cycle of the IFS.

*Proof.* 1. If  $z_0$  is in  $\Lambda$ , there is a  $k_1$  with  $z_0 \in g_{k_1}(\Lambda)$ . Thus  $g_{k_1}^{-1}(z_0) = z_1 \in \Lambda$ . There is a  $k_2$  with  $g_{k_2}^{-1}(z_1) = z_2 \in \Lambda$ , and so on. By the lemma, this sequence will enter the ball  $B_{2c}(0)$  after finitely many steps. Since  $\Lambda$  was closed and discrete, some  $z_j$  must appear a second time. 2. The equation says that for each  $x \in \Lambda$  the images  $g_k(x)$  must also be in  $\Lambda$ . So we get further points by application of the  $g_k$ . Since  $\Lambda$  is closed and discrete, the points will be outside  $B_{2c}(0)$  after finitely many steps. In all further steps,  $|g_k(y)| > |y| + d$  with  $d = g_k(\frac{\max |z_j|}{|\beta|})$  by the last assertion of Lemma 3. So each iteration of the  $g_k$  increases the distance from the origin by at least  $d$ , and the algorithm produces a discrete set in the plane. 3. This is true since all cycles of the expanding IFS lie in a bounded set. 4. Take the union of all solutions. It could be empty if we make no further assumptions on  $L$ . 5. This follows from 2. and 4.  $\square$

Note that cycles do not always come in isolated form. They often have a network structure, as discussed in Section 8. When we are within a discrete set, however, we can start with the union of all cycles and recursively apply the IFS to obtain the maximal solution of (4). This is how we shall construct our set  $\Lambda^*$ . However, we have not proved yet that the cycle network of the IFS  $\{g_1, \dots, g_m\}$  is discrete. This will be done by the cut-and-project method, and we have to require that  $\beta$  is a Pisot unit, so that  $1/\beta$  is an algebraic integer and  $g_k^{-1}(z) = (z - z_k)/\beta$  is defined as a mapping on  $R$ .

## 5 The contracting IFS and the attractor window

We fix a Galois automorphism  $x' = \varphi(x)$ . Then the expanding IFS (1) with  $g_k(z) = \beta z + z_k$  has the conjugate IFS  $g'_k(z) = \beta' z + z'_k$  for  $k = 1, \dots, m$ . Since  $\beta$  is a Pisot number, this IFS is contracting, that means  $|\beta'| < 1$ . When we consider this IFS on the complex plane, it has a unique fractal attractor  $A$ , defined by  $A = \bigcup g'_k(A)$  [7, 8, 9]. We assume that  $A$  has interior points. This condition is not critical. It will be fulfilled if we choose sufficiently many mappings so that the  $g'_k(A)$  cover a ball. We do not mind overlaps.

Let us complete the definition of the cut-and-project scheme which we began in Section 3. We take  $A \subset \pi'(\mathbb{Z}^d)$  as the window of our cut-and-project scheme and define the model set of the window  $A$  which has a very nice homogeneity properties. The following theorem holds for bounded windows  $A$  with interior points. Let

$$\Lambda(A) = \{x \in \pi(\mathbb{Z}^d) \mid x' \in A\} . \quad (7)$$

**Theorem 5 (Fundamental theorem on model sets [23, 18, 24, 4, 26, 30])**

1.  $\Lambda(A)$  is uniformly discrete (there is a minimal distance  $r > 0$  between the points).
2. If  $A$  has non-empty interior,  $\Lambda(A)$  is relatively dense (for some  $R > 0$ , the balls of radius  $R$  around its points cover the plane), and
3.  $\Lambda(A)$  is a Meyer set, that is, the difference set  $\Lambda(A) - \Lambda(A)$  is also uniformly discrete.
4. If  $\text{int } A \neq \emptyset$  and the area of the boundary of  $A$  is zero,  $\Lambda(A)$  has pure point diffraction spectrum [4, Theorem 9.4].

Now we can turn to the proof of Theorem 1. The main argument is the conjugacy of the expanding and contracting IFS:

$$(g_k(x))' = g'_k(x') \quad \text{for all } k = 1, \dots, m \text{ and } x \in R. \quad (8)$$

**Proposition 6 (Conjugates of discrete self-similar sets)**

- (i) For each cycle  $\{x_1, \dots, x_n\} \subset R$  of the expanding IFS  $g_1, \dots, g_m$ , the conjugate points  $x'_1, \dots, x'_n$  form a cycle of the contracting IFS  $g'_1, \dots, g'_m$ , and all the points  $x'_j$  belong to the attractor  $A$ .
- (ii) For each solution of the equation  $\Lambda = \bigcup g_k(\Lambda)$  in  $R$ , the conjugate set  $\varphi(\Lambda) = \{x' \mid x \in \Lambda\}$  is a dense subset of the attractor  $A$ .
- (iii) There are only finitely many solutions of (4) in  $R$ , and the union of these solutions is the maximal solution  $\Lambda^*$ .

*Proof.* (i). The correspondence of cycles follows directly from (8). A cycle of the contracting IFS fulfils  $g'_{j_n} \cdots g'_{j_1}(x_1) = x_1$ . So  $x_1$  belongs to  $A$  since it is the fixed point of the mapping  $g'_{j_n} \cdots g'_{j_1}$ , and the images  $x_2 = g'_{j_1}(x_1)$  etc. also belong to  $A$ . (ii). By Proposition 4.2, a solution  $\Lambda$  is obtained by starting with the cycle points  $x_i$  and repeatedly applying the  $g_k$ . The conjugate starting points  $x'_i$  are in  $A$ , and the conjugate maps  $g'_k$  are applied by (8), which means that the conjugate points remain in the attractor. Since each composition  $g'_{k_n} \cdots g'_{k_1}$  is used in the procedure, for any  $n$ , the set of points will become dense in  $A$ . (iii). This follows from Proposition 4 since all solutions are in the model set  $\Lambda(A)$  which is discrete by Theorem 5.  $\square$

For Theorem 1 it only remains to show that all points of  $\Lambda(A)$  belong to a solution of the equation (4). This is done in the next section.

## 6 Product attractor and finiteness

Fractal attractors often have an intricate structure. For that reason, we choose a ball  $B_{c'}(0) \supset A$  as an auxiliary window. The following choice of the radius  $c'$  will be used for Proposition 9.

**Lemma 7** *Let  $c' = \frac{\max_i |z'_i|}{1-|\beta'|}$ . Then  $|y| > c'$  implies  $|(g'_k)^{-1}(y)| > |y|$  for  $k = 1, \dots, m$ .*

*Proof.*  $|y| > c'$  means  $|y| - \max |z'_i| > |\beta'| \cdot |y|$ , and  $|(g'_k)^{-1}(y)| = \frac{|y-z'_k|}{|\beta'|} \geq \frac{|y| - \max |z'_i|}{|\beta'|}$ .  $\square$

We now switch to the general case of a Pisot number  $\beta$  with several conjugate roots or pairs of complex-conjugate roots  $\beta_1, \beta_2, \dots, \beta_q$ , where for a pair of complex roots we take only the  $\beta_k$  with positive imaginary part. For each  $\beta_j$  we let  $A_j \subset \mathbb{C}$  be the attractor of the contracting IFS  $g_k^j(x) = \beta_j x + z_k^j, k = 1, \dots, m$  which corresponds to the expanding IFS (1) under the Galois automorphism  $\varphi^j$  with  $\varphi^j(\beta) = \beta_j$ . In particular,  $z_k^j = \varphi^j(z_k)$ . The window under these circumstances is the product set  $A_1 \times \dots \times A_q$ , and the definition (7) of the model set generalizes to

$$\Lambda(A_1 \times \dots \times A_q) = \{x \in \pi(\mathbb{Z}^d) \mid \varphi^j(x) \in A_j \text{ for } j = 1, \dots, q\}. \quad (9)$$

For each  $j$ , we choose a ball  $B_{c_j}(0) \supset A_j$  with  $c_j = \frac{\max_i |z_i^j|}{1-|\beta_j|}$ , according to Lemma 7.

The purpose of the cut-and-project method in our approach is to determine the cyclic part of  $\Lambda^*$ . The rest of  $\Lambda^*$  is then constructed by iteration of the  $g_k$ . Lemma 3 says that the cyclic part of  $\Lambda^*$  is contained in the ball  $B_c(0)$ .

**Proposition 8** *Only a finite subset of  $R$  and of  $\mathbb{Z}^d$  is involved in the cut-and-project calculation of the cyclic part of  $\Lambda^*$ . Formally,*

$$F = \{n \in \mathbb{Z}^d \mid \pi(n) = x \in B_{2c}(0) \text{ and } \pi^j(n) = \varphi^j(x) \in B_{c_j}(0) \text{ for } j = 1, \dots, q\} \quad (10)$$

*is a bounded subset of  $\mathbb{Z}^d$ . In other words, it is contained in the set  $\mathbb{Z}_N^d$  defined in (5), for some positive integer  $N$ .*

*Proof.* We have here a finite-dimensional vector space  $V = \mathbb{C}^d \supset \mathbb{Z}^d$  and projections  $\pi, \pi^j = \varphi^j \pi$  onto complementary subspaces. Actually the basic map  $g(x) = \beta x$  can be written as the action of the companion matrix of the polynomial  $p$  on  $V$ , and the projections can be interpreted as projections onto the eigenspaces of that matrix. When a set has bounded projections in each of the subspaces, it must itself be bounded. The simplest argument uses compactness: any sequence in the set has a subsequence for which the projections in the subspaces converge. Then the subsequence itself must also converge.  $\square$

In the sections 4 and 5 we proved that a point  $x \in R$  belongs to  $\Lambda^*$  if and only if a finite sequence of inverse maps  $g_k^{-1}$  lead  $x$  to a cycle. A similar statement can now be given for the product attractor in the direct sum of contracting eigenspaces. For  $x \in R$ , let  $y = (y_1, \dots, y_q)$  with  $y_j = \varphi^j(x)$ . Actually we should write  $y = y_1 + \dots + y_q$  in order to underline that  $y \in R$ . Our notation focusses on the componentwise application of the contracting IFS  $\{g_k^j\}$  for  $j = 1, \dots, q$ .

**Proposition 9** 1. Let  $x \in R$ . The conjugate point  $y = (y_1, \dots, y_q)$  with  $y_j = \varphi^j(x)$  belongs to the attractor  $A_1 \times \dots \times A_q$  if and only if there are indices  $k_1, \dots, k_p \in \{1, \dots, m\}$  such that  $(g_{k_p}^j)^{-1} \dots (g_{k_1}^j)^{-1}(y_j)$  belongs to a cycle of the IFS  $\{g_1^j, \dots, g_m^j\}$  for every  $j = 1, \dots, q$ . The indices defining the cycle must be the same for all  $j$ .

2.  $\Lambda^* = \Lambda(A_1 \times \dots \times A_q)$ .

*Proof.* 1. We apply an arbitrary sequence of  $g_{k_i}^{-1}, i = 1, 2, \dots$  with  $k_i \in \{1, \dots, m\}$  to  $x$ . By Lemma 3 the resulting point  $x_\ell = g_{k_\ell}^{-1} \dots g_{k_1}^{-1}(x)$  is in  $B_{2c}(0)$  after a finite number  $\ell$  of steps and will stay there in all following steps. Now there are two cases. Either  $x_\ell, x_{\ell+1}, \dots$  all belong to the set of  $\pi(F)$  defined in (10). Then one of the  $x_i$  must appear a second time since the set is finite. In this case we have found a cycle for the  $g_k$ . By the conjugacy rule  $\varphi^j(g_k(x)) = g_k^j(\varphi^j(x))$ , which also holds for inverses, this yields a cycle for the maps  $g_k^j$  for each  $j$ . As in the proof of Proposition 6, we conclude that each  $y_j$  belongs to  $A_j$ , and  $y$  belongs to the product attractor. The second case is that some  $x_i$  with  $i \geq \ell$  does not belong to  $\pi(F)$ . Since  $x_i$  is in  $B_{2c}(0)$ , the definition of  $F$  implies that  $\varphi^j(x_i)$  is outside  $B_{c_j}(0)$  for some  $j$ . Further iteration by the  $(g_k^j)^{-1}$  will not lead back because of Lemma 7. So in this case  $y_j$  is outside  $A_j$ , and  $y$  is outside  $A_1 \times \dots \times A_q$ .

2. We actually proved that  $y$  belongs to the product attractor if and only if  $x$  belongs to  $\Lambda^*$ , according Proposition 4, 5. This completes the proof of Proposition 9 and of Theorem 1.  $\square$

## 7 The algorithmic approach

The construction of  $\Lambda^*$  involves three steps which we shall describe in detail for the case of a single attractor  $A$ .

1. Determine a finite set  $F_0 \subset R$  which contains the cyclic part of  $\Lambda^*$ .
2. Clean this set to obtain the proper subset  $F_1 = F_0 \cap \Lambda^*$ .
3. Recursively extend  $F_1$  to  $\Lambda^* \cap B_\rho(0)$  for a given bound  $\rho > 0$ .

**Step 1.** We know from Lemma 3 that we can assume  $F_0 \subset B_c(0)$  with  $c = \frac{\max_j |z_j|}{|\beta| - 1}$ . We choose a  $c'$  such that  $B_{c'}(0) \supset A$ . The value of Lemma 7 is admissible, and in the pentagonal example it is a good choice. Next, we determine an integer  $N$  with

$$\{n \in \mathbb{Z}^d \mid \pi(n) = x \in B_c(0) \text{ and } \pi'(n) \in B_{c'}(0)\} \subset \mathbb{Z}_N^d. \quad (11)$$

Proposition 8 says that such  $N$  exists. Now  $N$  must be really small, since  $\mathbb{Z}_N^d$ , defined in (10), contains  $\nu = (2N + 1)^d$  vectors which should fit into our computer. At this point the problem can turn out to be intractable, in particular for Pisot numbers of large degree  $d$ .

For small  $N$ , the rest of the calculation will cause no difficulties. We set up the Galois correspondence between points  $\pi(n)$  and  $\pi'(n)$  by calculating the  $2 \times \nu$  matrices  $X$  and  $X'$  described in Section 3. Then we select those columns  $\begin{pmatrix} x_{1,k} \\ x_{2,k} \end{pmatrix}$  of  $X$  which have modulus smaller

than  $c$ , and for which the corresponding columns  $\begin{pmatrix} x'_{1,k} \\ x'_{2,k} \end{pmatrix}$  of  $X'$  have modulus smaller than  $c'$ . These vectors form the set  $F_0$ .

**Recursive extension.** This algorithm will already be applied in step 2. We want to find the  $g_k$ -images of the given initial points, and the  $g_k$ -images of the new points, and so on, as long as their modulus is not larger than  $\rho$ . We know from Proposition 4 that there are only finitely many such points. However, we have to care for the overlaps. Since we get the same point several times, we must search and remove duplicates, which then can pop up again. We better construct our list  $L$  of points, a  $2 \times n$  matrix, point by point.

We start with the initial list  $L = \{z_1, \dots, z_{n_0}\}$  and set  $j = 1$  and  $n = n_0$ . Our working index  $j$  will never exceed the number  $n$  of points in the set  $L$ . When  $j > n$ , the program stops.

So suppose that we have  $L = \{z_1, \dots, z_n\}$  and  $j \leq n$ . Then we consider the  $m$  successors  $g_1(z_j), \dots, g_m(z_j)$ . For each of these points we first check whether it is in our list  $L$ . Only if it is not in the list, and its modulus is not greater than  $\rho$ , we add the point as  $z_{n+1}$  to our list and increase  $n$  by 1. Then we take the next successor. If all successors of  $z_j$  have been considered, we increase the working index  $j$  by 1, and take the new  $z_j$ , unless  $j > n$ .

**Step 2.** We apply the recursive extension to the set  $F_0$  with  $\rho = c$ , with the following modification. The list  $L$  is extended by  $m + 1$  further columns. We store for each  $z_\ell$  the column indices of the  $m$  successors  $g_k(z_\ell)$  which is done at the step  $j = \ell$ . In the last row of column  $\ell$ , we store the number of predecessors of  $z_\ell$ . Thus the last row is initially zero. Whenever  $z_\ell = g_k(z_j)$  for some  $j \geq 1$  and some  $k \in \{1, \dots, m\}$ , the last entry of column  $\ell$  is increased by 1. In the step 2 the recursive extension algorithm will not find new points. It is used to acquire information on successors and predecessors.

Now we consider all points of the list which have no predecessor. According to Proposition 4, they do not belong to  $\Lambda$ . These columns will be removed. However, before we remove one of them, we first go to its successors (given in rows 3 to  $m+2$ ) and decrease their predecessor number in the last row by 1. After removal of the columns we will have new points without predecessors. We repeat the procedure until all remaining points have at least one predecessor. Then the criterion 5. of Proposition 4 is fulfilled, and our set of points is  $F_1 = \Lambda \cap F_0$ .

**Step 3.** We apply the recursive extension algorithm to  $F_1$  and the given  $\rho$ , for instance  $\rho = 30$  for Figure 3 below. The successor numbers will not be stored. However, the number of predecessors will be kept for each point because it is used for the decoration of the points. Since the  $g_k$  are invertible maps, each point can have at most  $m$  predecessors, and at least one.

## 8 The basic pentagonal example

The algorithm will now be demonstrated for the example introduced in Section 1:  $g_k(x) = \tau x + z^k, k = 1, \dots, 5$  with  $\tau \approx 1.618$  and  $z = z^1 = e^{2\pi/5}$ . As mentioned in Section 3, the basis is taken as  $\{z, z^2, z^3, z^4\}$ . The Galois automorphism  $x' = \varphi(x)$  is defined by  $\varphi(z) = z^2$ . Since  $\tau = 1 + z + \bar{z}$ , we have  $\varphi(\tau) = -t$  with  $t = \tau - 1 = 1/\tau$ . Thus the conjugate system is  $g'_k(x) = -tx + z^k, k = 1, \dots, 5$ . The constant of Lemma 3 is  $c = \frac{1}{|\tau|-1} = \tau$ , and Lemma 7 gives  $c' = \frac{1}{1-|t|} = \tau^2 = 1 + \tau$ .

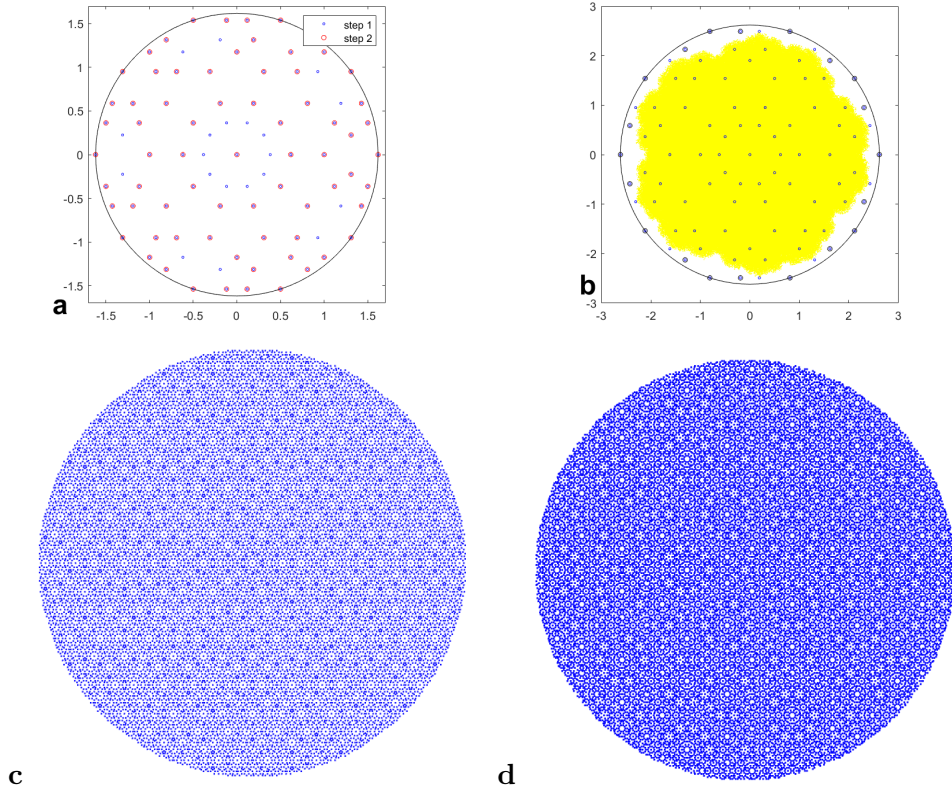


Figure 3: **a** shows the first two steps in the construction of the basic pentagonal pattern. The 91 points were projected from the ball around the yellow attractor  $A$  in the conjugate window **b**. The 71 points approved in the step 2 are circled in red. They include the cyclic part of  $\Lambda^*$ . The other 20 points do not belong to  $\Lambda^*$ . They correspond to the thick black points outside  $A$  in **b**. In step 3, the pattern was extended to the ball with radius  $\rho = 30$  in **c** and  $\rho = 40$  in **d**.

Now we determine the number  $N$  for (11). A simple experimental method is to determine for  $N = 1, 2, \dots$  the number of  $n$  with  $\pi(n) \in B_c(0)$  and  $\pi'(n) \in B_{c'}(0)$  and check where this number stabilizes. In this particular example  $N = 2$  is sufficient. We provide an analytical argument which will apply to all the examples below.

**Lemma 10** *For the cyclotomic field generated by  $z^1, \dots, z^4$  and arbitrary  $c$  and  $c'$ , the coordinates  $n_1, \dots, n_4$  in (11) fulfil*

$$4 \sum_i n_i^2 - 2 \sum_{i < j} n_i n_j = \sum_i n_i^2 + \sum_{i < j} (n_i - n_j)^2 \leq 2(c^2 + c'^2). \quad (12)$$

*Proof.* Putting  $\alpha = \pi/5$ , the basis vectors can be expressed with  $\alpha$  and  $2\alpha$ . A point  $u = \pi(n_1, n_2, n_3, n_4)$  has the form  $u = n_1 e^{2i\alpha} - n_2 e^{-i\alpha} - n_3 e^{i\alpha} + n_4 e^{-2i\alpha}$ . We calculate  $|u|^2 = u\bar{u}$ .

$$|u|^2 = n_1^2 + n_2^2 + n_3^2 + n_4^2 + 2 \cos 2\alpha (n_1 n_2 + n_2 n_3 + n_3 n_4) - 2 \cos \alpha (n_1 n_3 + n_2 n_4 + n_1 n_4)$$

The same can be done for the conjugate number  $u' = -n_1 e^{-i\alpha} + n_2 e^{-2i\alpha} + n_3 e^{2i\alpha} - n_4 e^{i\alpha}$ .

$$|u'|^2 = n_1^2 + n_2^2 + n_3^2 + n_4^2 + 2 \cos 2\alpha (n_1 n_3 + n_2 n_4 + n_1 n_4) - 2 \cos \alpha (n_1 n_2 + n_2 n_3 + n_3 n_4)$$

It is required that  $|u|^2 \leq c^2$  and  $|u'|^2 \leq c'^2$ . We ask how large the  $n_i$  can be if  $|u|^2 + |u'|^2 \leq c^2 + c'^2$ . Since  $\cos 2\alpha - \cos \alpha = -\frac{1}{2}$ , the term  $2(|u|^2 + |u'|^2)$  agrees with the left-hand side of (12).  $\square$

In our example,  $2(c^2 + c'^2) \leq 19$  while the smallest value of the left-hand side of (12) with  $n_1 = 3$ , say, is 24. So it is enough to consider  $N = 2$ , which involves  $\nu = 5^4 = 625$  vectors  $n$ . There are 91 cases for which  $\pi(n)$  is in  $U_c(0)$  and  $\pi'(n)$  in  $U_{c'}(0)$ . After the cleaning step 2 we are left with 71 points, shown in Figure 3a. The conjugates of the 20 points which we removed are in  $B_{c'}(0)$  outside the fractal attractor  $A$ , drawn in yellow in Figure 3b. It would have been more difficult to study the boundary of  $A$  and eliminate the points already in step 1. In step 3 we extended the set  $\Lambda^*$  to the circle around 0 with radius  $\rho = 30$ , containing more than 8000 points (Figure 3c).

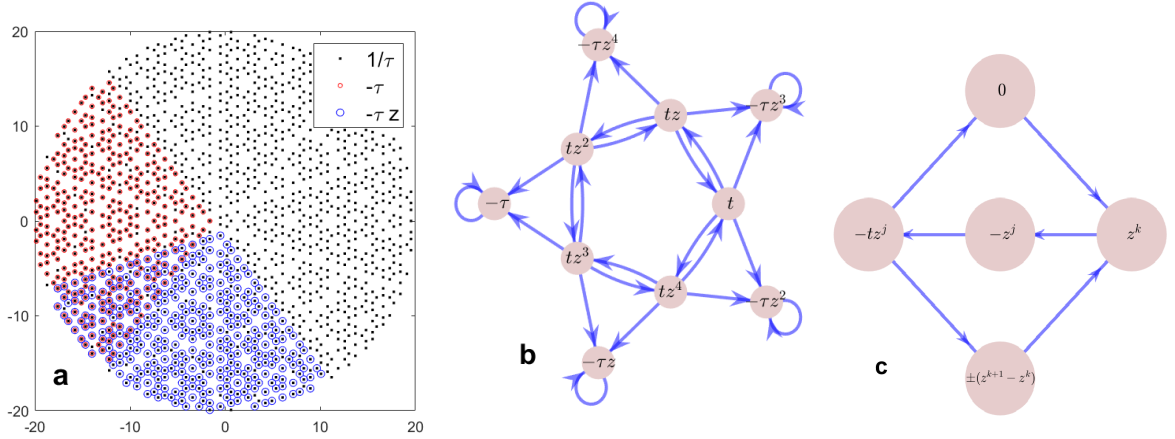


Figure 4: The recursive construction of  $\Lambda^*$  was applied in **a** to three different starting points. **b** shows the cycles established by the IFS between these points. **c** represents the larger component of the cyclic structure of  $\Lambda^*$ . Except for 0, each vertex stands for a group of 5 or 10 points.

We now discuss the structure of the cyclic part of  $\Lambda^*$ . The simplest cycles of the expanding IFS are the fixed points of  $g_k$ , the numbers  $-\tau z^k$  for  $k = 1, \dots, 5$ . When we recursively apply the IFS to one of these points, the resulting set is not relatively dense, as shown in Figure 4a for  $x_0 = -\tau$  (red set) and  $x_0 = -\tau z^1$  (blue set). Note that the two sets intersect although the initial cycles are disjoint. If we start with  $x_0 = 1/\tau = t$ , however, we obtain the black Meyer set which contains all red and blue points and many others. This is because the points  $tz^k, k = 1, \dots, 5$  form a two-sided cycle of the IFS, and the points  $-\tau z^k$  are obtained from them by application of the  $g_j$ , as indicated in Figure 4b. Vertices represent points, and there is an edge from  $x$  to  $y$  if  $g_k(x) = y$  for some  $k$ . Only the edges between cyclical points were drawn. The black generated set agrees with  $\Lambda_2$  in Figure 2b.

If we start with  $x_0 = 0$ , or with one of the  $z^k$  or  $-z^k$ , however, we get the Meyer set of Figure 2a. This is because the  $\pm z^k$ , the  $-tz^k$ , zero and the  $\pm(z^{k+1} - z^k)$  form an irreducible network which is explained in Figure 4c. Here each vertex stands for one group of points, and an edge from vertex  $u$  to vertex  $v$  is drawn if an image under some  $g_k$  from each point of the group  $u$  is contained in the group  $v$ . For instance  $g_k(0) = z^k$ . We did not specify which  $g_i$  maps  $-tz^j$  to which  $\pm(z^{k+1} - z^k)$  since it would be confusing to draw the graph of all 26 points.

So the cyclic part of  $\Lambda^*$  in this case consists of two components of 10 and 26 points, and the other 35 red points in Figure 3a are all images of the component of zero under repeated application of the  $g_k$ . We note that if we extend the IFS by the mapping  $g_0(x) = \tau x$ , as was done in [14], we get the same set  $\Lambda^*$ . It then can be generated from one initial point, say  $t$ , because  $g_0(t) = 1$  is in the other component. Our algorithm does not care for such details. It includes all cycles, without regard of the cyclic structure.

## 9 The decoration by the number of predecessors

Decorations play an important part in the study of aperiodic order [4, 12]. Markers are used to indicate matching rules for tiles, colors can indicate their orientation or type, or their Voronoi cells [14, 16]. In some way, all decorations reflect the local structure of a tiling or discrete set.

In our recursive construction of a self-similar discrete set  $\Lambda$ , there is a natural decoration which need not be invented - it comes for free. This is the number of predecessors  $x$  which a point  $y$  in  $\Lambda$  has - the number of  $k \in \{1, \dots, m\}$  for which there is a representation  $y = g_k(x)$ . This number is at least 1 and at most  $m$ , the number of mappings. Let us discuss the meaning of this decoration.

Each number  $x$  has  $m$  successors  $y_k = g_k(x) = \beta x + z_k, k = 1, \dots, m$ . They have a typical shape which characterizes the IFS and the point set  $\Lambda^*$ . Beside the Pisot factor  $\beta$ , the  $z_k$  are the only parameters which determine  $\Lambda^*$ . In our basic example  $\beta = \tau$  and the  $z^k$  form a pentagon. Now if a point  $y$  is the image  $y = g_j(x_j)$  for some  $j$ , the pentagon around  $\tau x_j$  with points  $\tau x_j + z^k, k = 1, \dots, 5$  must belong to  $\Lambda^*$ . Each point  $y$  belongs to at least one such pattern which we call cluster even though its points are not neighbours.

If  $y$  has the maximal number of five predecessors, however, it belongs to five such clusters. This case is shown in Figure 5a. The five clusters, drawn in yellow, green and grey, must form two decagons around  $y$ , with radius  $\sqrt{1+t^2} \approx 1.18$  and  $\sqrt{\tau^2+1} \approx 1.9$ , respectively, the length of a side and a diagonal of the pentagon. Thus  $y$  can be considered a local centre of symmetry of the point pattern. In our case, there are two more decagons around  $y$  with radius  $t$  and 1, for which we have no proof. In Figure 5b it can be seen that these decagons exist around all points with 5 predecessors which were marked red.

Regardless of symmetry, it seems correct to say that points with maximal number of predecessors are central and important places in the pattern. This is analogous to network analysis where vertices with a lot of links are considered as hubs or most central spots in the network. In Figure 5, each point has at least one parent and four siblings, but  $y$  has five parents and twenty siblings which puts  $y$  into a stronger position. It is also apparent that the shortest distance, which is  $t^3$ , the side length of tiny pentagons, is never realized by the red points. There may be one, two or even three neighbors at distance  $t^2$ , but not  $t^3$ . This can be proved.

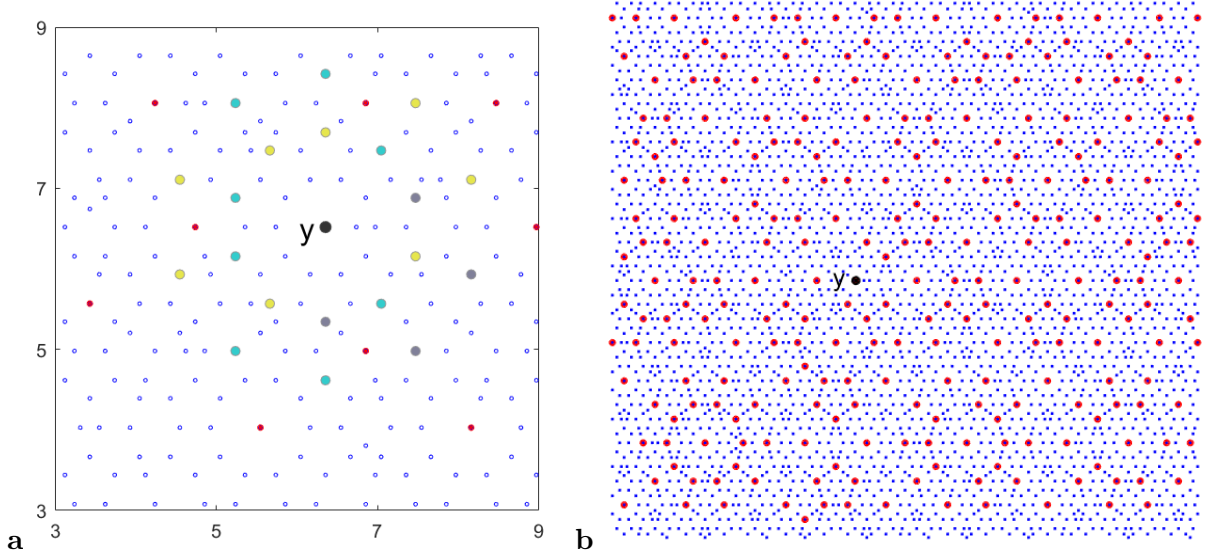


Figure 5: The point  $y$  in **a** has the maximal number 5 of predecessors. The 20 siblings surround  $y$ , forming two nested decagons. Such points can be considered as local symmetry centers. **b** shows on larger scale that these points, circled in red, constitute a more uniform substructure with clear pentagons and decagons.

**Proposition 11** *Let  $\Lambda$  be a solution of (4), where the IFS (1) has  $m$  mappings and factor  $\beta$ . Let  $\delta$  denote the minimum distance of neighboring points in  $\Lambda$ . If  $y$  has  $m$  predecessors, its distance to each other point  $x$  is at least  $\delta \cdot |\beta|$ . If  $y$  has  $m - j$  predecessors, at most  $j$  points can have distance  $\leq \delta \cdot |\beta|$  from  $y$ .*

*Proof.* Take  $\bar{x}$  with  $\beta\bar{x} + z_k = x$ . Then  $|y - z_k - (x - z_k)| = |y - x|$ , and  $\bar{y} = g_k^{-1}(y) = (y - z_k)/\beta$  fulfils  $\delta \leq |\bar{y} - \bar{x}| = |y - x|/\beta$ . If  $y$  had  $m - j$  predecessors and  $j + 1$  neighbors with distance  $\leq \delta \cdot |\beta|$ , we would find one  $x$  and  $k$  for which the argument applies.  $\square$

This explains why larger dots for points with greater number of parents fit into the figure without covering neighbors. There is an analogy to physical quasicrystals which are alloys of Aluminium (Al), with atomic weight 27, with heavier metals like Cu, Co, Mn, Ni, or Fe, all with atomic weight larger 50. The larger atoms are smaller in number. In our patterns, points with large number of predecessors appear in similar percentage as heavy atoms in physical quasicrystals.

The number of predecessors can also be characterized by associated regions of the window. A point  $y$  has  $\ell$  predecessors if and only if its conjugate point  $y'$  belongs to  $\ell$  pieces  $g'_k(A)$  of the attractor  $A$ . Thus, unless there is extreme overlap, the number of points with  $m$  predecessors is rare. In Figure 1, the tiny pentagon in the centre represents the intersection of all pieces. It occupies  $(t^4)^2 \approx 2\%$  of the area of  $A$ .

Our experience is that the decoration provides insight into the structure of  $\Lambda^*$ , as below in Section 11. On the other hand not every number of predecessors has a special meaning, and

the subjective choice of coloring and size of the points influences the appearance. We never use more than four colors, and mostly prefer a decent decoration by red circles just for the maximum number of predecessors.

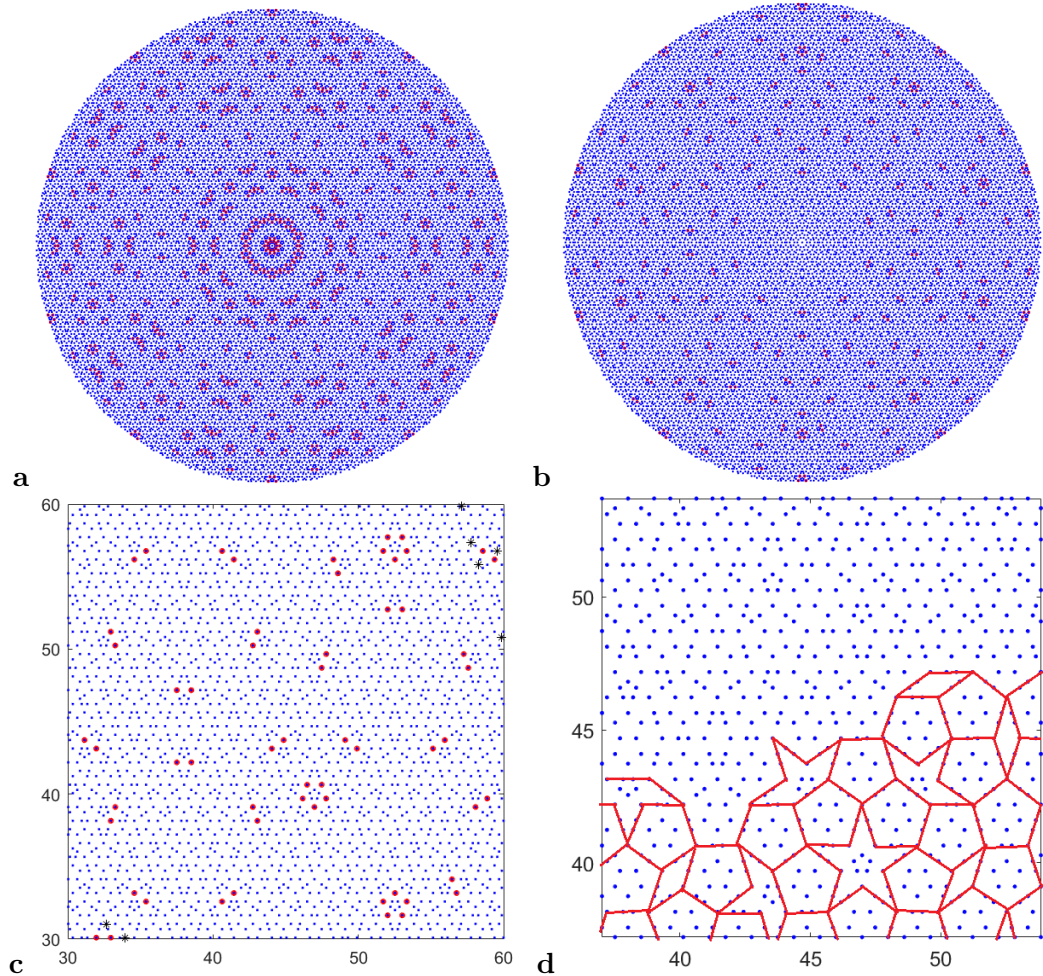


Figure 6: **a.** The decagonal pattern of Hare, Mazakova and Vavra for  $\rho < 50$ . **b.** For the initial point 0 we obtain the model set of  $\text{int } A$  which looks more homogeneous. **c.** Far from the origin, both patterns coincide on larger and larger regions. Here the model set with the window  $A$  contains just 7 more points, indicated by black stars. **d.** Part of **c** with Penrose P1 tiles [12, Figure 10.3.3] showing that the patch belongs to the Penrose class.

## 10 Compact or open window? Go away from the origin!

The decagonal model set of Hare, Masakova und Vavra [14] is based on  $m = 11$  mappings with factor  $\tau^2 \approx 2.618$ . Besides  $g_0(x) = \tau^2 x$ , they took the tenth roots of unity:  $g_k(x) = \tau^2 x + z^k$  and

$g_{k+5}(x) = \tau^2 x - z^k, k = 1, \dots, 5$ . The conjugate IFS consists of  $g'_0(x) = t^2 x$  and  $g'_k(x) = t^2 x \pm (z')^k$ . We are still in the cyclotomic field generated by the fifth roots of unity. The conjugacy  $(z^k)' = z^{2k}, k = 1, \dots, 5$  applies as  $z' = z^7$  to all tenth roots  $z = \pm z^k$ . The attractor  $A$  is a decagon with fractal boundary inside the convex hull of the points  $\pm \tau z^k$  which as fixed points of the  $g'_k$  belong to  $A$ . The bounds are  $c' = \tau$  and  $c = t$ . In Lemma 10 the right-hand side equals 6, so  $N = 1$  is sufficient for our algorithm. The cyclical part of  $\Lambda^*$  consists just of the fixed points of the  $g_k$ , that is,  $\pm t z^k$  and 0. Their conjugate points are on the boundary of the attractor, except for zero. The model set in Figure 6a is rather inhomogeneous, in particular near the origin.

This example can be modified by taking the open set  $\text{int } A$  as the window, that is, starting the recursion algorithm only with the initial point 0. The resulting pattern in Figure 6b looks more coherent but the neighborhood of 0 is still special, due to the fixed point 0. A much better solution is to observe the pattern far from the origin where both versions coincide on larger and larger patches. See Figure 6, c and d. Only in this view it turns out that  $\Lambda^*$  is related to the Penrose tilings.

**Remark 12 (Draw self-similar patterns far from their cyclical part)** *A self-similar point pattern, as given by (4) or by a self-similar tiling or ‘geometrical substitution’, is commonly drawn in a neighborhood of the origin. Such figures are misleading when near to zero there are algebraic integers on the boundary of the window. In that case the origin is a rather untypical point of the model set. The general picture of patches is revealed when we go far from the origin, which is possible by our algorithm.*

Of course, this was just an observation which will be confirmed in the next section. It would be nice to have rigorous estimates for regions where the model sets of  $A$  and  $\text{int } A$  coincide. In concrete cases, however, this can be checked by calculation.

## 11 A very coherent decagonal pattern

Figure 7 visualizes a new IFS with expanding factor  $\tau^2$ . We extend the contracting maps  $g'_k(x) = t^2 x + z^k, k = 1, \dots, 5$  by  $g'_{k+5}(x) = t^2 x - \tau z^k$  and do not include  $g'_0$ . The fixed points  $\tau z^k$  and  $-\tau^2 z^k$  form a decagonal star. Figure 7a shows the resulting area-filling attractor  $A$ . Applying conjugacy, and neglecting a permutation of the indices  $k$ , the expanding mappings are  $g_k(x) = \tau^2 x + z^k$  and  $g_{k+5}(x) = \tau^2 x + t z^k$ , with fixed points  $-t z^k$  and  $-t^2 z^k$ , respectively. The bounds are  $c = t$  and  $c' = \tau^2$ . Lemma 10 shows that  $N = 2$  is sufficient for the projection step.

The 21 points of the projection to  $B_c(0)$  are shown in Figure 7b. The five small blue points do not belong to the cyclical part of  $\Lambda^*$ . Their conjugates are clearly outside the attractor. If the recursion is applied to the remaining 16 points, we obtain Figure 7c. It has some dense spots with points of very small distance.

For this IFS we cannot take  $\text{int } A$  as a window. When we remove all cyclic points with conjugates on the boundary, no cyclic part is left. Only the red points 0 and  $t z^k$  have conjugates in the interior of  $A$  and therefore must be included in the recursion. The points  $-t z^k$  circled in black, the fixed points of the  $g_k$ , have conjugates on the boundary of  $A$ . The same is true for the red points  $-t^2 z^k$  on the inner circle. They are the fixed points of the  $g_{k+5}$ . However, they map to 0, and 0 maps to the  $t z^k$  which are not cyclic themselves. Thus to take an open window,

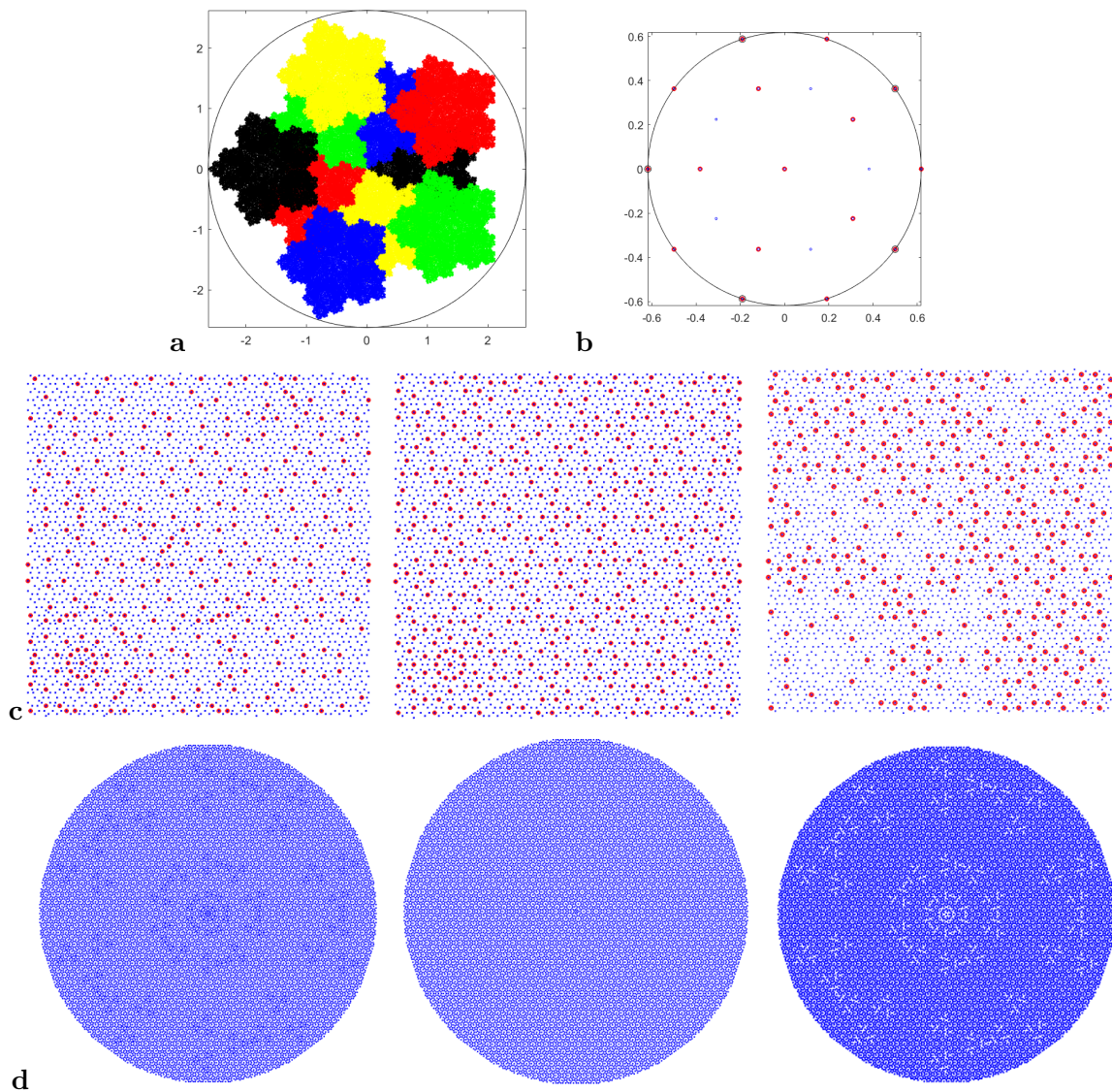


Figure 7: **a.** The attractor of the conjugate IFS. **b.** The 16 red points contain the cyclical part of  $\Lambda^*$ . The small blue points have conjugates outside  $A$ . **c.** The model sets of  $A$  (left) and of  $\text{int } A$  (right), and a set in-between obtained from the initial value 0, all for  $-3 < x_1, x_2 < 12$ . **d.** The same sets for  $\rho < 36$ . On the left, overpopulated areas look dark. On the right, underpopulated spots form white filaments. The example in the middle is the most homogeneous one.

omitting the inner circle, we have to include  $g_0(x) = \tau^2 x$  in the IFS in order to make 0 a cyclic point. The result of applying the recursion only to 0 is shown in Figure 7d. There are some spots which look somewhat empty.

A very interesting modification is shown in Figure 8a. We excluded the points  $-tz^k$  circled

in black in Figure 7b, but included the red points on the inner circle as initial points. This defines a model set  $\Lambda(B)$  with  $\text{int } A \subset B \subset A$ . We had to add  $g_0(x) = \tau^2 x$  to the IFS in order to obtain a relatively dense set  $\Lambda$ . The result is an extremely coherent pattern, shown in Figure 8b with full decoration. The macrostructures in Figure 8c verify this coherence.

Note that the maximal number of predecessors in Figures 6, 7 and 8 is three, with exception of the point 0. Rather few points with three predecessors are centres of pentagons or decagons since the attractors have relatively small overlap.

This section went far into detail to show that beyond the model set and self-similarity properties, there are differences in the geometric appearance which can be regulated by slightly changing the IFS and the window.

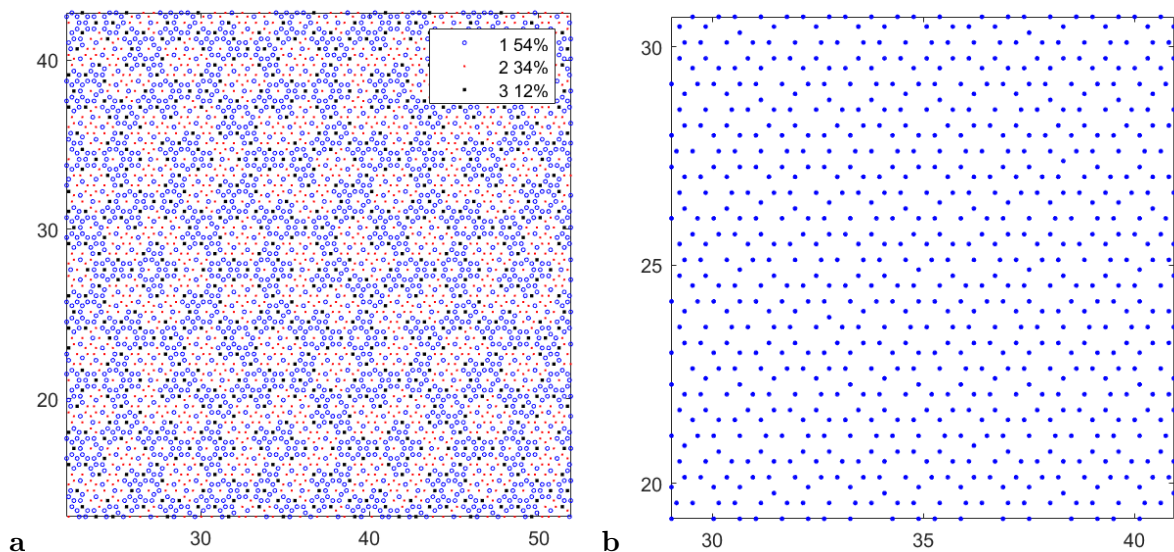


Figure 8: A regular view. Far from zero all three versions coincide. **a.** The decoration emphasizes the macrostructure. **b.** A part of **a** without decoration. None of the small decagons is complete.

## 12 Further examples

We restrict ourselves to a few more examples. First we replace the basic IFS  $g_k(x) = \tau x + z^k$  by  $g_k(x) = \tau x + 2z^k$ . This is equivalent to studying the basic IFS on  $R/2$  instead of  $R$ . The new solution set will have higher density, and will contain the basic solution set as a subset. The bounds of Section 8 are doubled:  $c = 2\tau$  and  $c' = 2\tau^2$ . A larger part of  $\mathbb{Z}^d$  needs to be considered. The right-hand side of Lemma 10 is now 76, which yields  $N = 5$ . (For  $n_1 = 6$ , say, the smallest value of the left-hand side would be  $36 + 6 \cdot 9 = 90$ .) Thus we have to consider  $\nu = (2 \cdot 5 + 1)^4 = 14641$  algebraic integers in the projection step. Almost 1000 lattice points project to the two circles in physical and internal space, and 900 survive the cleaning step 2 of the algorithm, as indicated in Figure 9a,b.

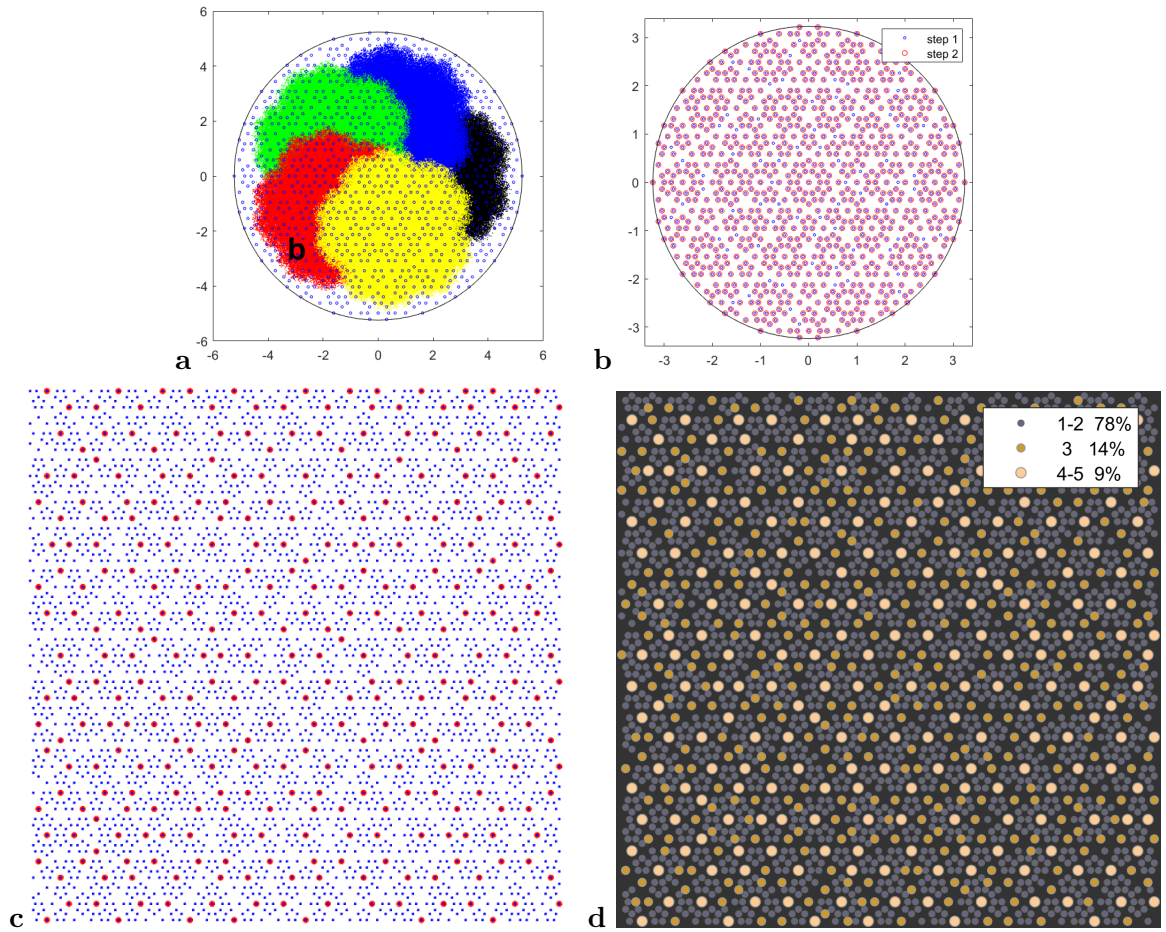


Figure 9: **a.** The attractor of  $g'_k(x) = -tx + 2z^k$  with almost 1000 algebraic integers which have their conjugates in  $B_c(0)$ . **b.** Step 2 of the algorithm removes less than 100 points. The remaining 900 points contain the cyclical part of  $\Lambda^*$ . **c.** The resulting pattern has four times higher density and is shown here for  $-2 < x_1, x_2 < 10$  while similar pictures above fulfilled  $-4 < x_1, x_2 < 21$ . We can see “empty streets”. **d.** The same picture with full decoration on slightly smaller scale.

The resulting Meyer set  $\Lambda^*$  in Figure 9c,d shows “empty streets”, apparent already in Figure 9b. They reflect the lattice directions and alternate with parallel streets full of points. We are not on a sublattice, however. We have a full model set  $\Lambda^*$ . Compared with the other examples, the set has double density both in  $x_1$  and  $x_2$ -direction. We magnified  $\Lambda^*$  in order to allow comparison with Figures 7 and 8.

There is an infinity of choices for the factor  $C \in \mathbb{Z}[\tau]$  in  $g_k(x) = \tau x + Cz^k$  although only few of them lead to a tractable  $N$ . For  $C = \tau^n, n \in \mathbb{Z}$  we get our basic example with another density. When we rescale both axes with factor  $1/C$ , we obtain exactly the basic example. Thus when we factor  $\mathbb{Z}[\tau]$  by  $u \sim v$  if  $v = u\tau^n$ , it is sufficient to take one parameter from each equivalence class.

Besides  $C = 3, 4, \dots$  we can take values like  $C = 2 + \tau, 3 - \tau, \dots$ . Since the attractors do basically coincide, all versions have the same relative density of points with  $j = 1, \dots, 5$  predecessors. A similar modification of the examples of Section 11, where the  $z_k$  are on two different circles, produces a lot of other patterns with essentially different attractors.

So far we studied only IFS with factor  $\tau$  or  $\tau^2$ . Now let us consider the  $g_k(x) = -\tau x + z^k$  with their conjugate mappings  $g'_k(x) = tx + z_k, k = 1, \dots, 5$ . They generate the pentagon attractor of Figure 1. The bounds are  $c = \tau$  and  $c' = \tau^2$  as in Section 8, so the first step of the algorithm is the same. In the step 2, five more points are assigned to  $\Lambda^*$ . Figure 10 shows  $\Lambda^*$  which is a bit different from previous examples

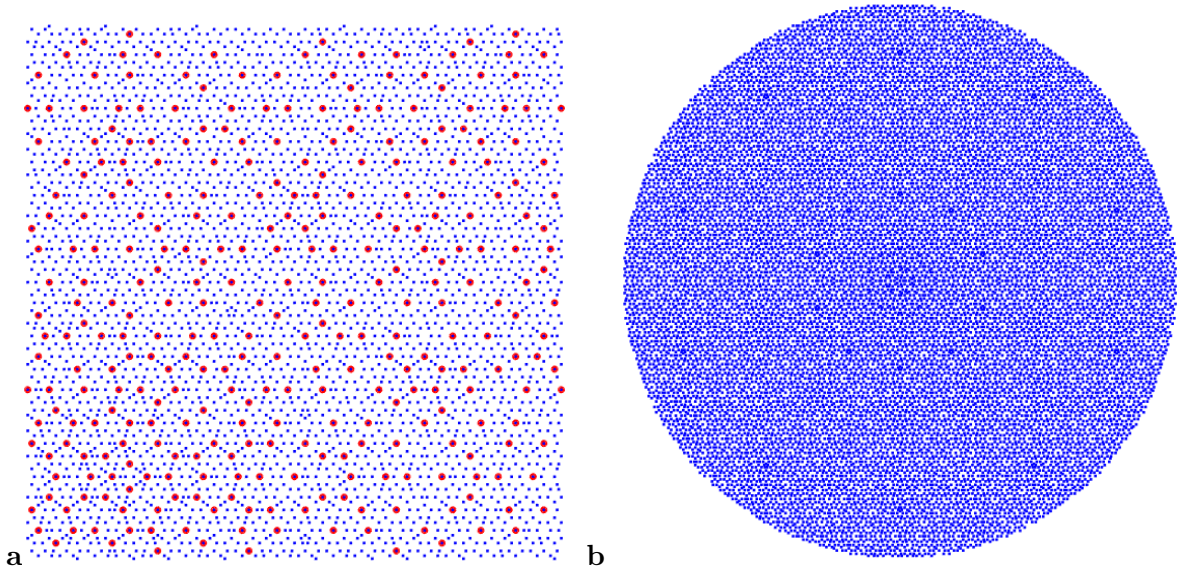


Figure 10: **a.**  $\Lambda^*$  for  $g_k(x) = -\tau x + z^k$ . **b.** View for  $\rho \leq 30$ . Compared with Figure 3c, there is less large-scale structure, except for a few little dark spots, most of them near to the origin.

All modifications for the factor  $\tau$  can also be applied to the factor  $-\tau$ . Moreover, there is no need to choose the  $z_k$  as an  $n$ -gon on a circle, which opens up a huge box of other examples. When we take four maps  $g_k(z) = \tau z + z_k$ , for instance, with  $z_k = 0, 1, z, z^{-1}$  where  $z$  is a fifth root of unity, the attractor  $A$  still has interior points. The resulting patterns look less symmetric than the above figures and seem to have larger holes. On the other hand, when we take complex Pisot units like  $\tau z$ , we get similar pictures as above.

**Conclusion.** We introduced a construction of self-similar cut-and-project model sets. We have focussed on the most simple examples with decagonal symmetry, because of their relation to physical quasicrystals. Even in this class our algorithm provides a lot of different model sets. To compare and sort all these examples, more research is necessary. We must determine difference sets, autocorrelation functions, and diffraction spectra, as well as other structural properties. Computer-assisted work is required to evaluate the models for possible use in physics and material science.

## References

- [1] E. Abe, Y. Yan, and S.J. Pennycook. Quasicrystals as cluster aggregates. *Nature materials*, 3(11):759–767, 2004.
- [2] S. Akiyama, Y. Nagai, and S.-Q. Zhang. Overlapping substitutions and tilings. *arXiv preprint arXiv:2407.18666*, 2024.
- [3] P. Arnoux, M. Furukado, E. Harriss, and S. Ito. Algebraic numbers, free group automorphisms and substitutions on the plane. *Trans. Amer. Math. Soc.*, 363(9):4651–4699, 2011.
- [4] M. Baake and U. Grimm. *Aperiodic Order, Vol. 1: A mathematical invitation*. Cambridge University Press, Cambridge, 2013.
- [5] C. Bandt. Self-similar tilings and patterns described by mappings. In R.V. Moody, editor, *The Mathematics of Long-range Aperiodic Order*, volume C 489 of *NATO ASI Series*, pages 45–84. Kluwer Academic Publishers, 1997.
- [6] C. Bandt. Elementary fractal geometry. 3. Complex Pisot factors imply finite type. *Discrete Comput. Geom.* 74:661-690, 2025.
- [7] B. Bárány, K. Simon, and B. Solomyak. *Self-similar and self-affine sets and measures*, volume 276 of *Mathematical Surveys and Monographs*. American Mathematical Society, 2023.
- [8] M.F. Barnsley. *Fractals everywhere*. Academic Press, 2nd edition, 1993.
- [9] K.J. Falconer. *Fractal geometry: mathematical foundations and applications*. J. Wiley & sons, 3 edition, 2014.
- [10] H. Ferru. Caractérisation des nombres de Pisot complexes. *Bull. Soc. Math. France*, 19:5–20, 1969.
- [11] D. Frettlöh, E. Harriss, and F. Gähler. Tilings encyclopedia. <https://tilings.math.uni-bielefeld.de/>, 2023.
- [12] B. Grünbaum and G.C. Shephard. *Patterns and Tilings*. Freeman, New York, 1987.
- [13] P. Gummelt. Penrose tilings as coverings of congruent decagons. *Geometriae Dedicata*, 62(1):1–17, 1996.
- [14] K.G. Hare, Z. Masáková, and T. Vávra. On the spectra of Pisot-cyclotomic numbers. *Letters in Mathematical Physics*, 108(7):1729–1756, 2018.
- [15] E. Harriss, H. Koivusalo, and J.J. Walton. When is a cut and project set substitutional? *arXiv preprint arXiv:2512.13659*, 2025.
- [16] T. Hejda and E. Pelantová. Spectral properties of cubic complex Pisot units. *Mathematics of Computation*, 85(297):401–421, 2016.

- [17] J.C. Lagarias and Y. Wang. Substitution Delone sets. *Discrete Comput. Geom.*, 29:175–209, 2003.
- [18] J.C. Lagarias. Geometric models for quasicrystals I. Delone sets of finite type. *Discrete & Computational Geometry*, 21(2):161–191, 1999.
- [19] J.-Y. Lee and B. Solomyak. Pisot family self-affine tilings, discrete spectrum, and the meyer property. *Discrete and Continuous Dynamical Systems*, 32(3):935–959, 2012.
- [20] R. Li, Z. Li, Z. Dong, and K.A. Khor. A review of transmission electron microscopy of quasicrystals—how are atoms arranged? *Crystals*, 6(9):105, 2016.
- [21] C. Liu, K. Kitahara, and A. Ishikawa et al. Quasicrystals predicted and discovered by machine learning. *Physical Review Materials*, 7:093805, 2023.
- [22] J. Masáková, J. Mazáč, and E. Pelantová. On generalized self-similarities of cut-and-project sets. *Linear Algebra Appl.*, 625:279–321, 2021.
- [23] Y. Meyer. *Algebraic numbers and harmonic analysis*, volume 2 of *North-Holland Mathematical Library*. North-Holland Publishing Company, Amsterdam and London, 1972.
- [24] R.V. Moody. Meyer sets and their duals. In R.V. Moody, editor, *The Mathematics of Long-range Aperiodic Order*, volume C 489 of *NATO ASI Series*, pages 403–441. Kluwer Academic Publishers, 1997.
- [25] M. Senechal. *Quasicrystals and geometry*. Cambridge University Press, Cambridge, 1995.
- [26] B. Solomyak. Delone sets and dynamical systems. *Substitution and Tiling Dynamics: Introduction to Self-inducing Structures: CIRM Jean-Morlet Chair, Fall 2017*, pages 1–32, 2020.
- [27] W. Steurer. Gummelt versus Lück decagon covering and beyond. implications for decagonal quasicrystals. *Acta Cryst.*, A77:36–41, 2021.
- [28] W. Steurer and S. Deloudi. Decagonal quasicrystals – what has been achieved? *C. R. Physique*, 15:40–47, 2014.
- [29] R.S. Strichartz. Fractals in the large. *Canadian Journal of Mathematics*, 50(3):638–657, 1998.
- [30] R. Yassawi and V. Berthé. Meyer sets, Pisot numbers, and self-similarity in symbolic dynamical systems. In *Documents Mathématiques*. Société Mathématique de France, 2024. arXiv:2404.04116v2.

Institute of Mathematics, University of Greifswald, Germany, [bandt@uni-greifswald.de](mailto:bandt@uni-greifswald.de)  
 Académie des Sciences, 23 quai de Conti, 75006 Paris, France, [yves.meyer305@orange.fr](mailto:yves.meyer305@orange.fr)